Electronic Supplementary Material (ESI) for Materials Horizons.
This journal is © The Royal Society of Chemistry 2022

Supporting Information

Polarization-perceptual Anisotropic Two-dimensional ReS_2 Neuro-transistor with Reconfigurable Neuromorphic Vision

Dingdong Xie[a,1], Kai Yin[a,1], Zhong-jian Yang[a], Han Huang[a], Xiaohui Li[b], Zhiwen Shu[c], Huigao Duan[c], Jun He[a,*], and Jie Jiang[a,*]

[a]Hunan Key Laboratory of Nanophotonics and Devices, School of Physics and Electronics, Central South University, 932 South Lushan Road, Changsha, Hunan 410083, P. R. China

[b]School of Physics and Information Technology, Shanxi Normal University, Xi'an 710119, China

[c]State Key Laboratory of Advanced Design and Manufacturing for Vehicle Body, College of Mechanical and Vehicle Engineering, Hunan University, Changsha 410082, People's Republic of China

[1] These authors contributed equally to this work.

E-mail: junhe@csu.edu.cn; jiangjie@csu.edu.cn

Experimental Section

Preparation of 2D ReS_2 sample. 2D multilayer ReS_2 flakes were firstly exfoliated from a bulk crystal by traditional Scotch-tape approach, and subsequently transferred to the heavily-doped silicon substrate with a thickness of 300nm thermally-grown SiO_2 dielectric layer.

Fabrication of ReS_2 phototransistor. The prepared ReS_2 sample was spin-coated with a thin film of photoresist (PR1-2000A1, Semi-LED (Beijing) Co., Ltd). Then, the drain/source electrodes with Au/Ni stack (60/10nm) were generated through ultraviolet lithography (365nm), thermal-evaporation (10^{-4}Pa), and lift-off process to obtain ReS_2 phototransistor.

Characterization of ReS_2 flakes. The ReS_2 profile thickness was extracted from AFM (NanomanVS+Multimode, Veeco). ARPRS measurement of ReS_2 was performed in a Renishaw Confocal Raman microscope (inVia Qontor).

Photoelectric measurements of ReS_2 neuro-transistor. The photoelectric performances and neural behaviors were observed by Keithley 4200 SCS with a relative humidity of 40% in the dark at room temperature. The polarized-light signals were performed using a fiber-coupled laser module with a wavelength of 860nm (MDL-III-860 nm-50 mW-19040407) and 552nm (MGL-FN-405 nm-50 mW-19040501).

Note S1. Fitting analysis of measurement results

1.1 *Fitting analysis of Raman peak intensity*

As shown in Fig. 1f-h (main text), the intensity of Raman peaks can be fitted in polar coordinates by the following equations

$$\delta(\alpha) = \delta_a \cdot \cos^2(\alpha+\beta) + \delta_b \cdot \sin^2(\alpha+\beta) \quad \text{(S1)}$$

$$\delta(\alpha) = \delta_a \cdot \cos^2(\alpha+\beta) + \delta_b \cdot \sin^2(\alpha+\beta) + \delta_c \cdot \cos^2(\alpha+\beta) \cdot \sin^2(\alpha+\beta) \quad \text{(S2)}$$

where α is the polarization angle, and δ_a, δ_b, δ_c, and β are the fitting parameters. The Raman intensity of E_g and A_g-like modes can be fitted by the eqn (S1), while the E_g-like modes can be fitted by the eqn (S2). The fitting results are summarized in Table S1.

1.2 *Fitting analysis of polarization-dependent degree*

The relationship between I_{max}/I_{min} and V_{GS} is shown in Fig. S5, which can be perfectly fitted by using an exponential decay model as the following equation

$$I_{max}/I_{min} = f(V) = A_1 \cdot \exp(\frac{-V}{V_1}) + A_\infty \quad \text{(S3)}$$

where A_∞, A_1, and V_1 are the ultimate value of I_{max}/I_{min}, the I_{max}/I_{min} amplitude, and the characteristic voltage constant, respectively. The fitting results of A_∞, A_1, and V_1 are 99.8%, 3.0%, and 23.2 V, respectively.

1.3 *Fitting analysis of ReS_2 absorptance*

The theoretical calculation of ReS_2 absorptance is shown in Fig. S7, which can be well fitted with the following equation

$$A_{bs}(\alpha) = A_{bs1} \cdot \cos^2(\alpha+\phi) + A_{bs2} \cdot \sin^2(\alpha+\phi) + A_{bs3} \cdot \cos^2(\alpha+\phi) \cdot \sin^2(\alpha+\phi) \quad \text{(S4)}$$

where α is the polarization angle, and A_{bs1}, A_{bs2}, A_{bs3}, and ϕ are the fitting parameters. The fitting results of A_{bs1}, A_{bs2}, A_{bs3}, and ϕ are 8.2%, 8.2%, 3.2%, and 84°, respectively.

1.4 *Fitting analysis of parameters A_-/A_+ and τ_-/τ_+*

As shown in Fig. 4f-i (main text), it is obvious that all the figures show the same four-lobed shape. The value of A_-/A_+ and τ_-/τ_+ can be fitted in polar coordinates by the same following equation

$$f(\alpha) = \mathrm{f_a} \cdot \cos^2(\alpha+\eta) + \mathrm{f_b} \cdot \sin^2(\alpha+\eta) + \mathrm{f_c} \cdot \cos^2(\alpha+\eta) \cdot \sin^2(\alpha+\eta) \qquad \text{(S5)}$$

where α is the polarization angle, and f_a, f_b, f_c, and η are the fitting parameters. The fitting results can be found in Table S8.

1.5 *Fitting analysis of parameters A, τ, W_0, and t_0*

As shown in Fig. 4j-m (main text), it is clearly seen that A, τ, and t_0 have the same two-lobed shape, while W_0 has four-lobed shape. These parameters can be fitted by the following sinusoidal equations

$$y(\alpha) = \mathrm{y_a} \cdot \cos^2(\alpha+\sigma) + \mathrm{y_b} \cdot \sin^2(\alpha+\sigma) \qquad \text{(S6)}$$

$$y(\alpha) = \mathrm{y_a} \cdot \cos^2(\alpha+\sigma) + \mathrm{y_b} \cdot \sin^2(\alpha+\sigma) + \mathrm{y_c} \cdot \cos^2(\alpha+\sigma) \cdot \sin^2(\alpha+\sigma) \qquad \text{(S7)}$$

where α is the polarization angle, and y_a, y_b, y_c, and σ are the fitting parameters. These parameters of A, τ, and t_0 can be fitted by the eqn (S6), while W_0 can be well fitted by the eqn (S7). The fitting results can be found in Table S9.

1.6 *Fitting analysis of parameters (b and k)*

As shown in Fig. 5f,g (main text), it is clearly observed that most of the data points are on the black fitting curve, indicating that these fitting results are very well. These parameters can be further fitted by the following equations

$$b(\alpha) = \mathrm{A_b} \cdot \exp\left(-\frac{(\alpha+\alpha_0)^2}{\tau_b^{\,2}}\right) + \mathrm{b_0} \qquad \text{(S8)}$$

$$k(\alpha) = \mathrm{k_a} \cdot \cos^2(\alpha+\zeta) + \mathrm{k_b} \cdot \sin^2(\alpha+\zeta) + \mathrm{k_c} \cdot \cos^2(\alpha+\zeta) \cdot \sin^2(\alpha+\zeta) \qquad \text{(S9)}$$

where α is the polarization angle, and A_b, b_0, α_0, τ_b, ζ, k_a, k_b, and k_c are the fitting parameters. The *y*-axis intercept (*b*) can be fitted by the Gaussian eqn (S8), while the slope (*k*) can be fitted by the sinusoidal eqn (S9). The fitting results of A_b, b_0, α_0, τ_b, ζ,

k_a, k_b, and k_c are −0.4 nA, 0.9 nA, −129.5°, 76.1°, −160°, 91.0 pA·s/spikes, 84.0 pA·s/spikes, and −183.4 pA·s/spikes, respectively.

Note S2. The calculations of responsivity and detectivity

According to previous reports, the responsivity (R) can be defined as: $R=I_{ph}/(PS)$, where I_{ph} is the photocurrent, P is power density of the incident light, and S is the effective area under illumination.[1] Indeed, our device exhibits an excellent R of ~8.3 A/W under 50 mW/cm^2 illumination at λ = 552 nm, V_{GS} = -30 V, and V_{DS} = 0.1V. Furthermore, the corresponding detectivity (D^*) can be calculated to be 2.3×10^8 Jones via the formula, $D^* = \frac{R\cdot\sqrt{S}}{\sqrt{2q\cdot I_{dark}}}$, where q is the electron charge and I_{dark} is the dark current.[1,2] For comparison, more performance details of a series of 2D-based photodetectors are listed in Table S5.

Note S3. The relationship between dichroic ratio and stimulus number

To further investigate the effect of polarized-light spike number on dichroic ratio, Fig. S14 shows the typical optical EPSCs and the extracted $EPSC_{Ave}$ under different V_m. From these figures, it is obvious that the optical EPSC increases with the increase of stimulus number, which may be caused by the superposition of photocurrent.[3,4] At the same time, the extracted $EPSC_{Ave}$ exhibit the same four-lobed shape and main polarization directions (70°, 160°, 250°, and 340°), which may be due to the in-plane vibrations of Re atoms[5,6]. Moreover, the $EPSC_{Ave}$ can be well fitted by the eqn (4) (main text). The fitting results are summarized in Table S7. As a result, the relationship among dichroic ratio, stimulus number and V_m can be further summarized, as shown in Fig. S15. It is clearly observed that the dichroic ratio increases with the increase of stimulus number with a fixed V_m. Furthermore, for a fixed stimulus number, the dichroic ratio would decrease when V_m becomes more negative. It is to be

noted that the dichroic ratio reaches a maximum value of ~198.8% at the stimulus number of 20 and V_m of −10 V.

Supplementary Figures

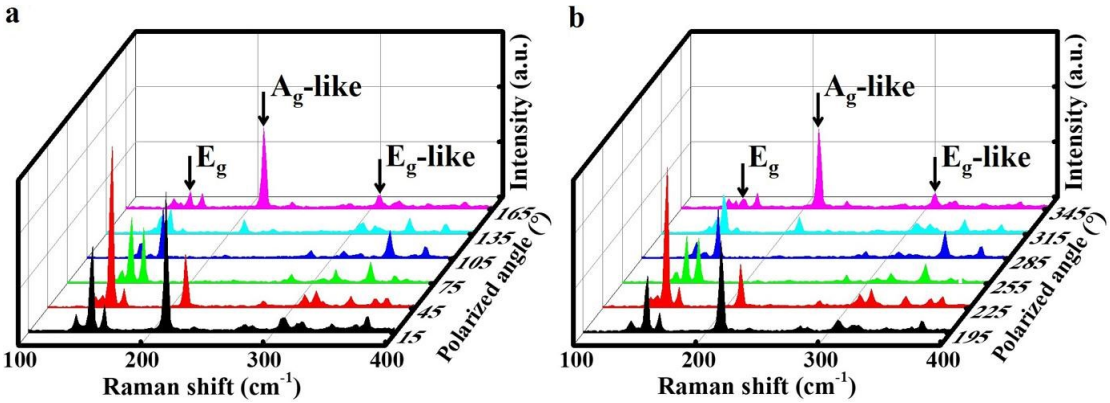

Fig. S1 ARPRS measurements of ReS_2. The Raman spectrum with three characteristic modes, E_g (152.8 cm^{-1}), A_g-like (212.6 cm^{-1}), and E_g-like (308.2 cm^{-1}) modes.

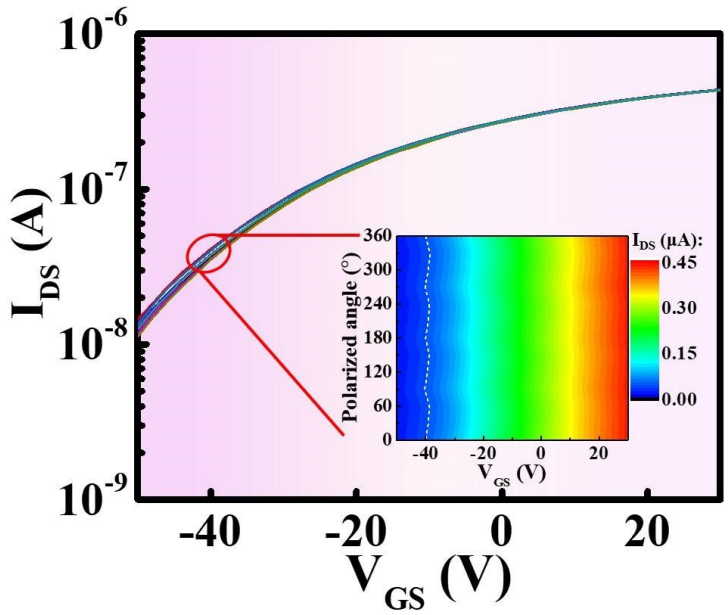

Fig. S2 I_{DS} as a function of V_{GS} derived from Fig. 2c (main text). These different colors of the solid line represent different polarization angles. Inset: the 2D colormap for the same Fig. 2c in main text.

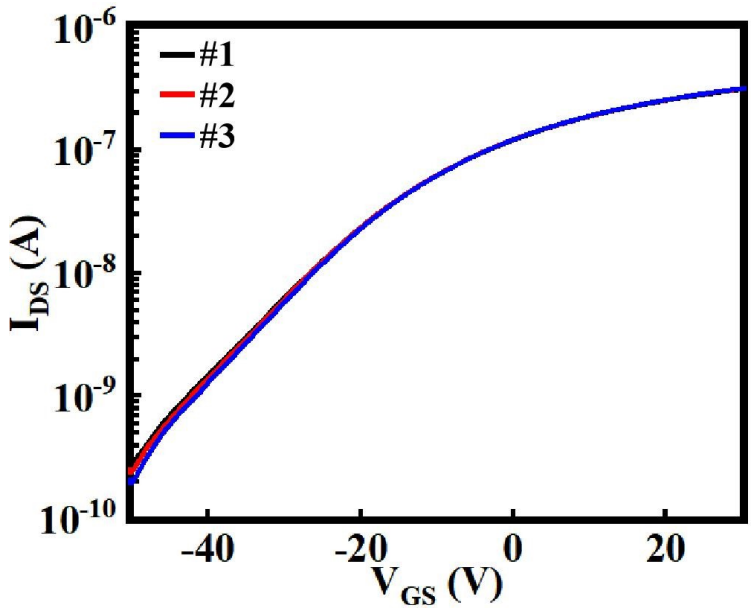

Fig. S3 Transfer curve of the ReS_2 phototransistor under the fixed bias of V_{DS}=0.1V for three successive measurements in the dark.

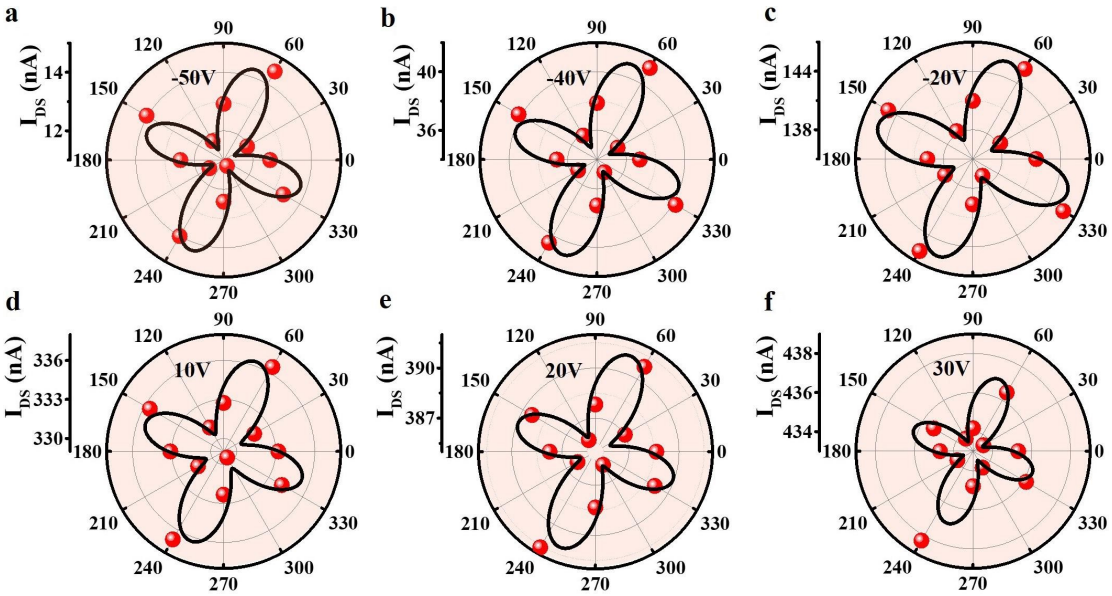

Fig. S4 Evolution of the extracted I_{DS} plotted in the polar coordinates under different V_{GS}. The V_{GS} changes from −50 V to 30 V, corresponding to Fig. (a-f), respectively. The red balls are the experimental values, while the black solid curves are the fitting results.

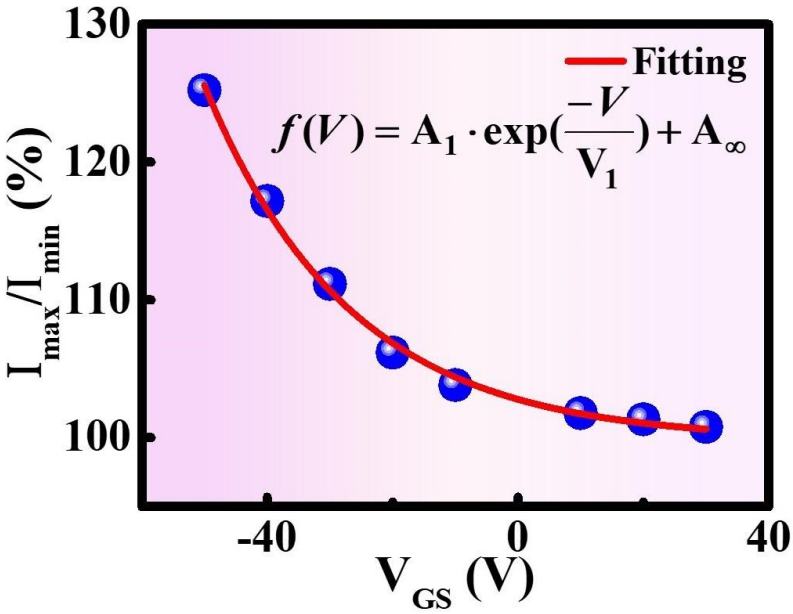

Fig. S5 I_{max}/I_{min} as a function of V_{GS}. The experimental data can be well fitted by an exponential equation.

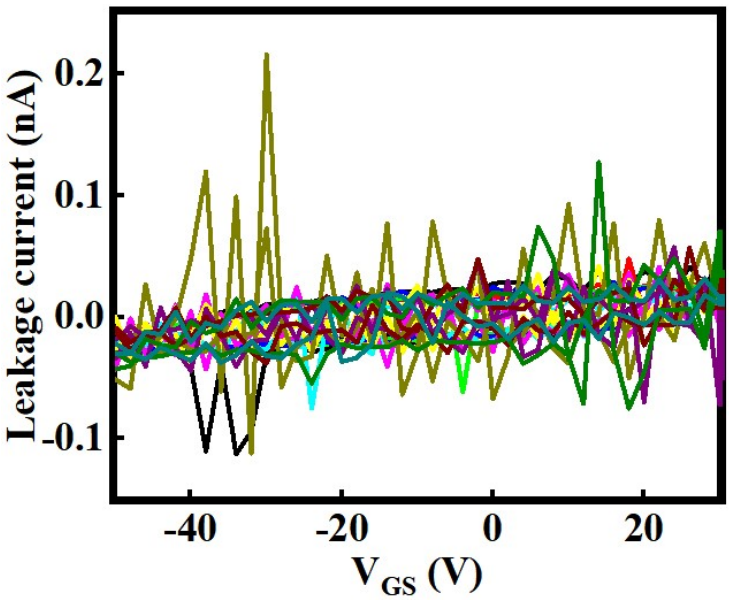

Fig. S6 The leakage current of the ReS_2 phototransistor for the voltage sweeping from −50 V to 30 V. These different colors of the solid line represent different polarization angles.

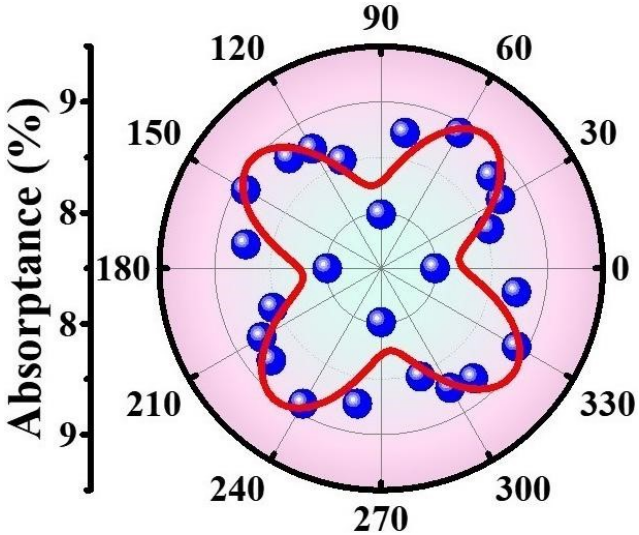

Fig. S7 Absorptance versus polarization angle in polar coordinates. Blue ball symbol is the extracted experimental data, while red solid curve is the fitting result.

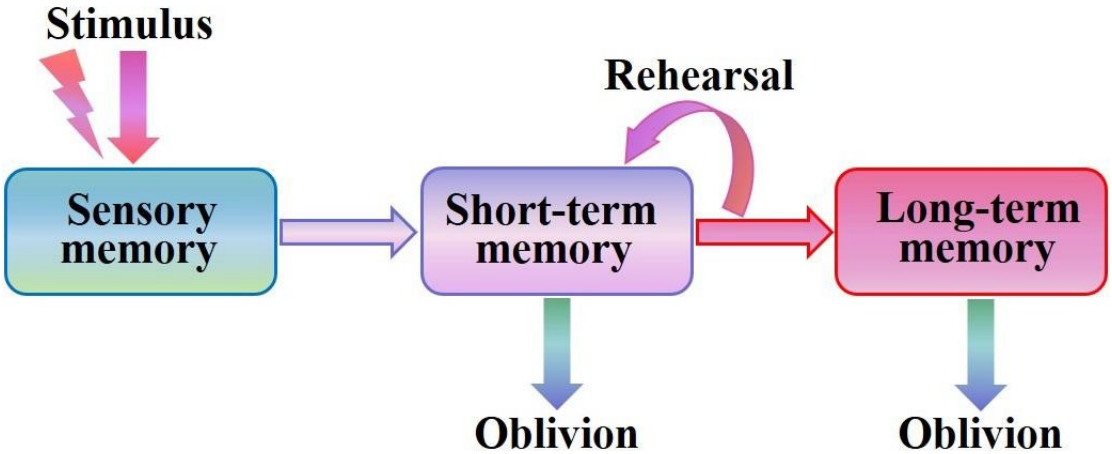

Fig. S8 Schematic diagram of the process of polarization memory consolidation.

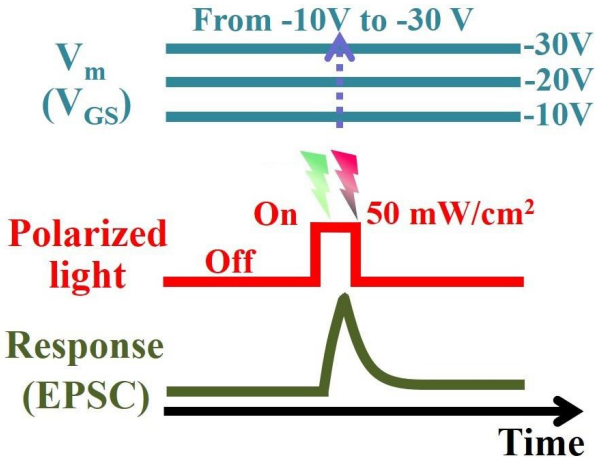

Fig. S9 Schematic diagram of measurement method of optical EPSC. All of the EPSC measurements are performed in the polarization-sensitive photodetection system (Fig. 2a, main text). We have two complete polarized-light testing systems with wavelengths of 552 nm and 860 nm. During the measurements, the polarized-light spike can be served as pre-synaptic input, while the ReS_2 channel current can be acted as post-synaptic response. Herein, the intensity of the polarized-light is fixed at 50 mW/cm^2. A fixed modulatory voltage (V_m) is applied to the bottom gate during the measurement. The V_m can be changed from −10 V to −30 V to regulate the EPSC response.

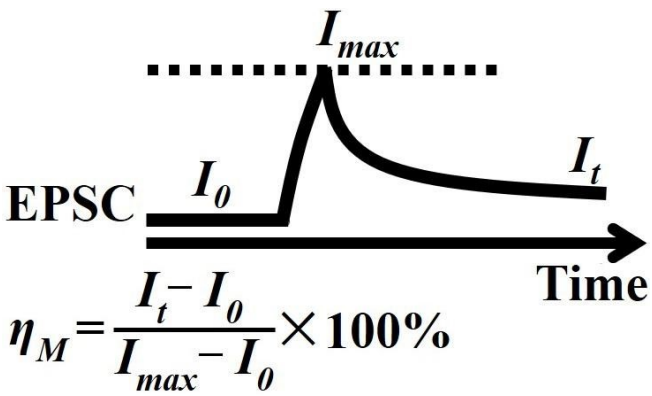

Fig. S10 The schematic diagram of the equation definition of η_M .

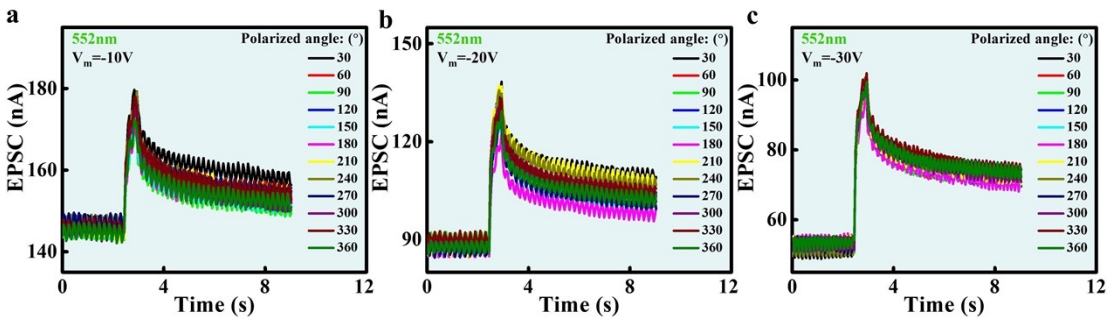

Fig. S11 The typical optical EPSCs response of ReS_2 neuro-transistor with different polarization angles (light wavelength: 552 nm, light power: 50 mw/cm^2, pulse duration: 0.5 s). It can be regulated by different V_m of −10 V (a), −20 V (b), and −30 V (c), respectively.

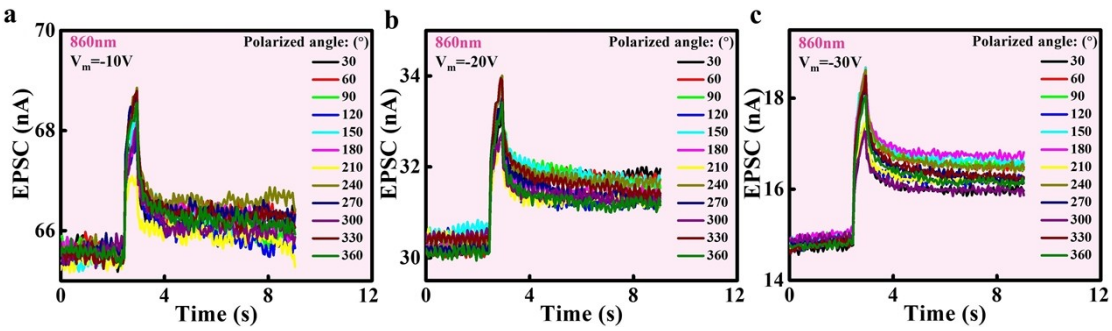

Fig. S12 The typical optical EPSCs response of ReS_2 neuro-transistor with different polarization angles (light wavelength: 860 nm, light power: 50 mw/cm^2, pulse duration: 0.5 s). It can be regulated by different V_m of −10 V (a), −20 V (b), and −30 V (c), respectively.

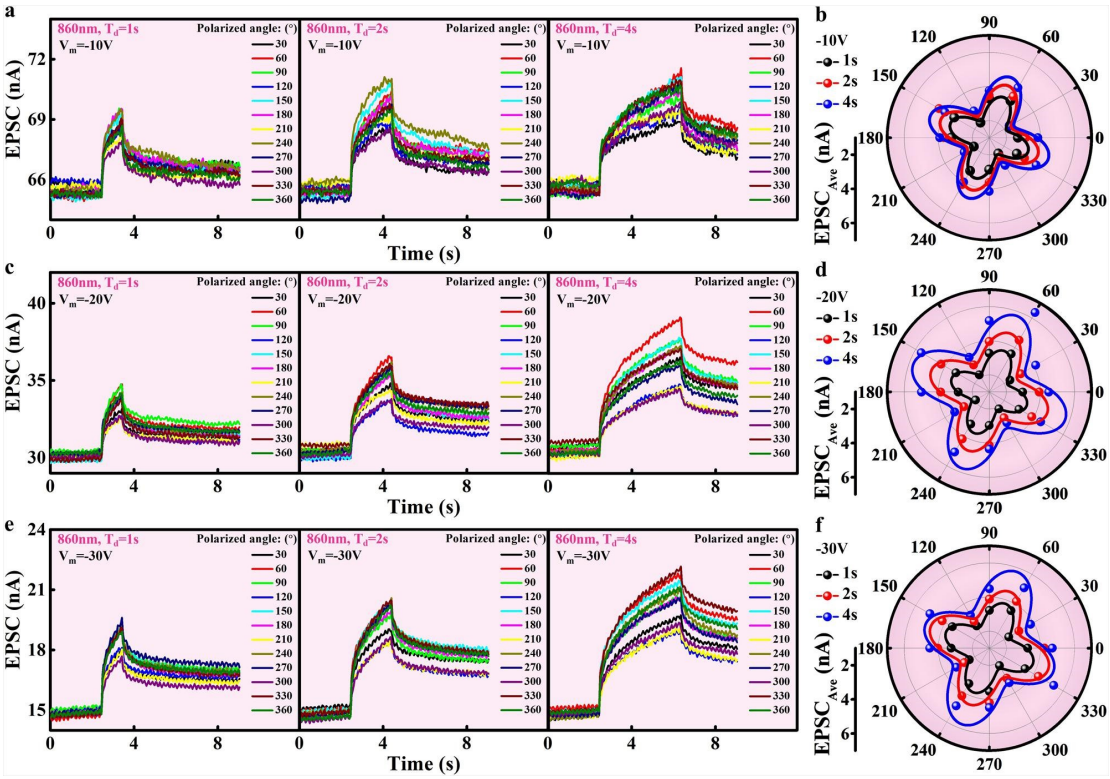

Fig. S13 The typical polarized response of optical EPSCs and the extracted $EPSC_{Ave}$ under different T_d and V_m. The polarization light is set with a light wavelength of 860 nm and light power of 50 mw/cm^2. Furthermore, T_d varies from 1 s to 4 s, and V_m changes from −10 V to −30 V, respectively. Herein, the extracted $EPSC_{Ave}$ can also be fitted by the eqn (4) (main text). The fitting results can be summarized in Table S6.

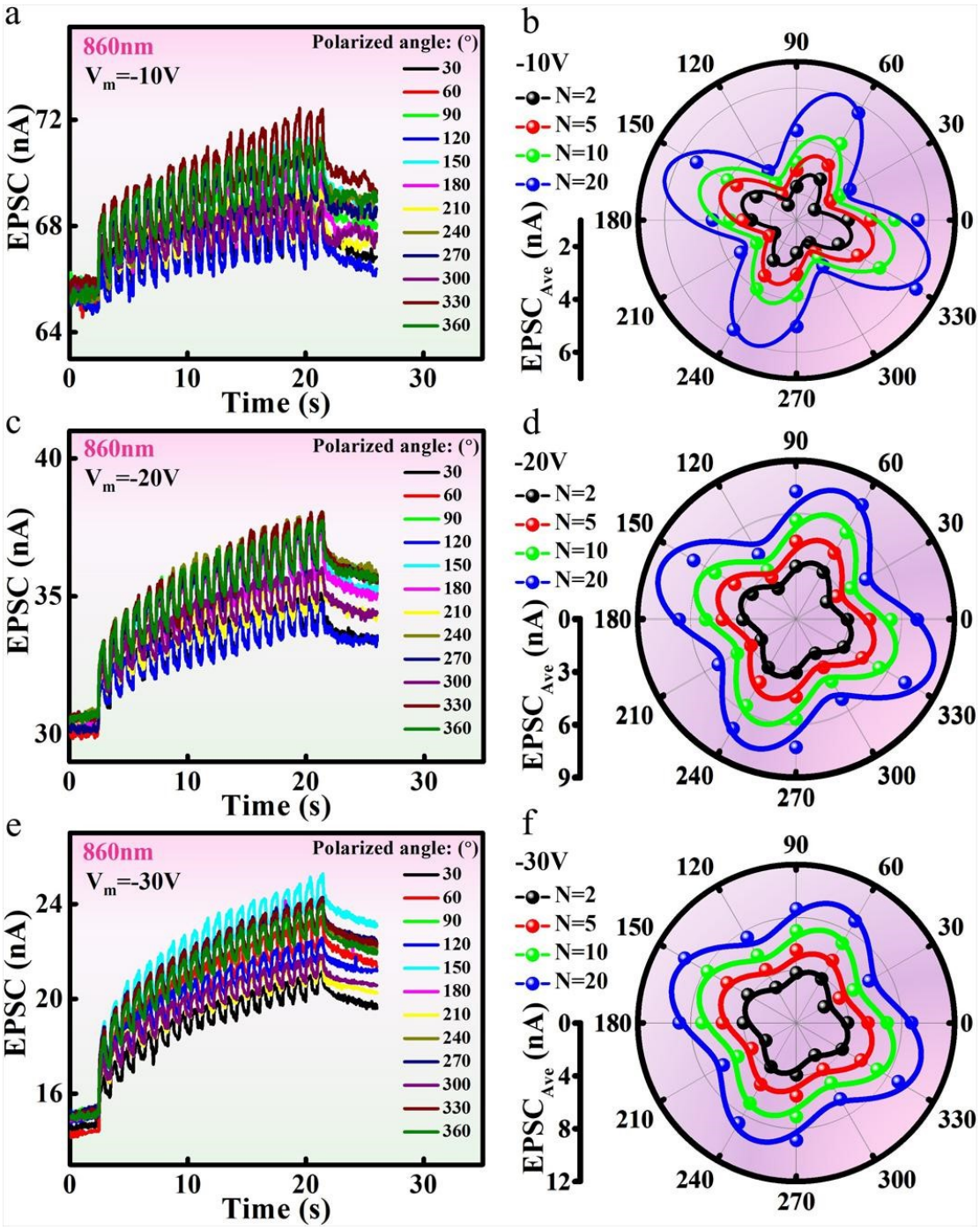

Fig. S14 The typical polarization response of optical EPSCs and the extracted $EPSC_{Ave}$ with V_m changing from −10 V to −30 V. The polarization light is set to (light wavelength: 860 nm, light power: 50 mw/cm^2, pulse duration: 0.5 s), and the total stimulus number is 20. Herein, the extracted $EPSC_{Ave}$ can be well fitted by the eqn (4) (main text). The fitting results can be summarized in Table S6.

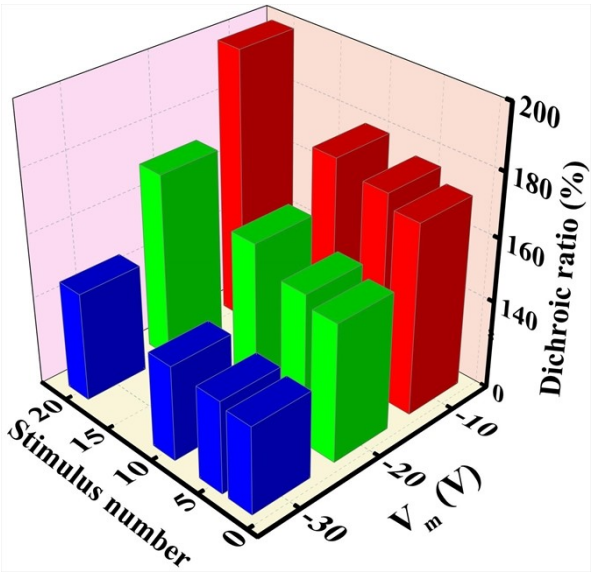

Fig. S15 Dichroic ratio as a function of stimulus number and V_m.

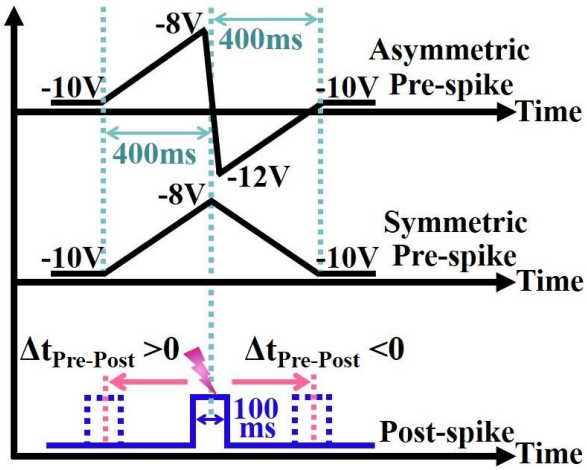

Fig. S16 STDP implementation schemes with programmed pre-spike and post-spike in ReS_2 neuro-transistor. During the measurements, the pre-spike (programmable voltage spike) is applied to the bottom gate, while the post-spike (polarized-light spike with 860 nm) is applied to the ReS_2 channel. The $\Delta t_{Pre-Post}>0$ indicates that the polarized-light spike is before the voltage spike, otherwise, $\Delta t_{Pre-Post} < 0$.

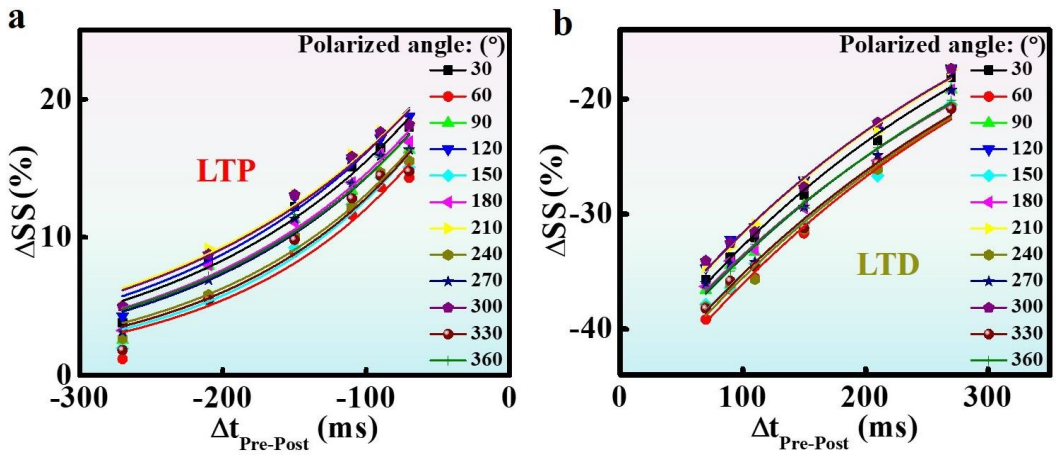

Fig. S17 A amplified image of Fig. 4d of main text.

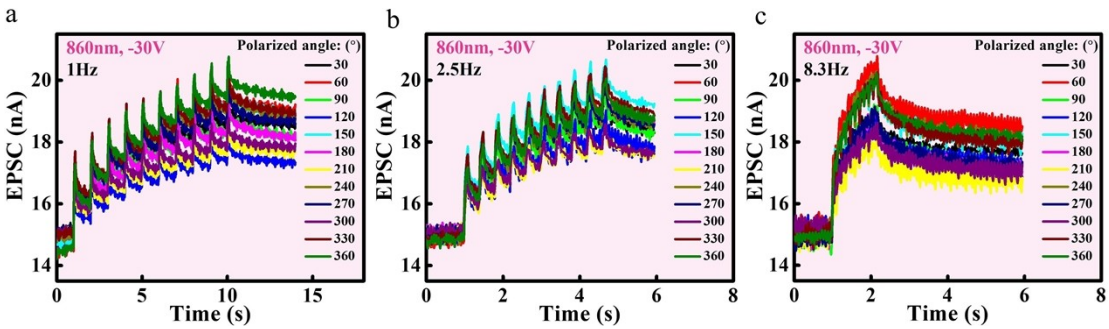

Fig. S18 The optical EPSCs are triggered by the polarized-light train under a fixed frequency of 1 Hz (a), 2.5 Hz (b), and 8.3 Hz (c) for different polarization angles, respectively. Each stimulus train consists of ten concessive polarized-light spikes (light wavelength: 860 nm, light power: 50 mw/cm^2, pulse duration: 0.5 s) under a fixed frequency and a fixed V_m of −30 V.

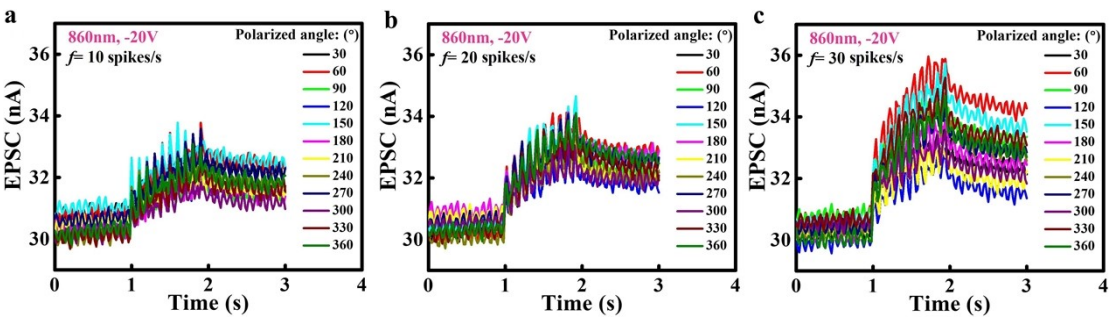

Fig. S19 The optical EPSC responses triggered by the polarized-light driving input (pulse duration：20 ms) under a mean rate of 10 spikes/s (a), 20 spikes/s (b), and 30 spikes/s (c) with different polarization angles, respectively. The polarization wavelength is 860 nm, while V_m is fixed at −20 V.

Supplementary Tables

Table S1. The summarized table of the fitting results (δ_a, δ_b, δ_c, and β) for the intensity of Raman peaks.

	δ_a	δ_b	δ_c	β (°)
E_g	2800.1	10.2	-	135
A_g-like	2200.3	10.1	-	165
E_g-like	292.9	193.9	-506.4	-35

Table S2. The summarized table of the fitting results (I_a, I_b, I_c, and χ) for I_{DS}.

V_{GS} (V)	I_a (nA)	I_b (nA)	I_c (nA)	χ (°)
-50	13.8	14.3	-10.5	-160
-40	39.9	40.9	-22.0	-160
-30	85.3	85.7	-33.6	-160
-20	145.3	145.6	-33.3	-160
-10	210.9	211.1	-30.7	-160
10	335.4	336.3	-21.6	-160
20	389.9	391.1	-18.1	-160
30	436.2	436.9	-12.1	-160

Table S3. The summarized table of the fitting results (I_{Pmax}, I_{Pmin}, and γ) for the extracted $EPSC_{Ave}$ in 552 nm polarized light.

V_{GS} (V)	I_{Pmax} (nA)	I_{Pmin} (nA)	γ (°)
-10	25.1	18.1	95
-20	38.0	28.1	95
-30	39.9	32.0	95

Table S4. The summarized table of the fitting results (I_{P1}, I_{P2}, I_{P3}, and γ) for the extracted $EPSC_{Ave}$ in 860 nm polarized light.

V_{GS} (V)	I_{P1} (nA)	I_{P2} (nA)	I_{P3} (nA)	γ (°)
-10	2.7	2.8	-4.1	-160
-20	2.9	2.8	-3.8	-160
-30	2.9	3.1	-3.7	-160

Table S5. Some recently reported 2D-based photodetectors and their performance parameters (N/A: not applicable).

Device	Responsivity (R)	Detectivity (D^*)	Ref.
$ReSe_2$	0.1 A/W at 633 nm	N/A	7
Sb_2Se_3	1.6 A/W at 633 nm	N/A	8
Td-$MoTe_2$	0.4 mA/W at 532 nm	1.1×10^8 Jones at 532 nm	9
β-$GeSe_2$	2.5 A/W at 450 nm	1.9×10^8 Jones at 450 nm	10
ReS_2	8.3 A/W at 552 nm	2.3×10^8 Jones at 552 nm	This work

Table S6. The summarized table of the fitting results (I_{P1}, I_{P2}, I_{P3}, and γ) for the extracted $EPSC_{Ave}$ in 860 nm polarized light with different T_d.

T_d (s)	V_{GS} (V)	I_{P1} (nA)	I_{P2} (nA)	I_{P3} (nA)	γ (°)
1	-10	3.4	3.5	-5.4	-160
	-20	3.3	3.6	-5.2	-160
	-30	3.7	3.8	-5.5	-160
2	-10	4.0	4.2	-6.8	-160
	-20	4.6	4.6	-7.3	-160
	-30	4.7	4.5	-6.7	-160
4	-10	4.7	4.7	-8.4	-160
	-20	5.7	5.7	-9.5	-160
	-30	5.0	5.7	-8.0	-160

Table S7. The summarized table of the fitting results (I_{P1}, I_{P2}, I_{P3}, and γ) for the extracted $EPSC_{Ave}$ in 860 nm polarized light with different stimulus number.

Stimulus number	V_{GS} (V)	I_{P1} (nA)	I_{P2} (nA)	I_{P3} (nA)	γ (°)
	-10	3.2	2.8	-4.5	-160
2	-20	3.3	3.4	-4.6	-160
	-30	4.1	4.0	-4.4	-160
	-10	4.0	3.5	-6.0	-160
5	-20	4.6	4.7	-6.8	-160
	-30	6.0	5.4	-5.8	-160
	-10	4.9	4.3	-7.5	-160
10	-20	5.9	6.2	-9.3	-160
	-30	7.7	7.3	-8.3	-160
	-10	6.3	6.0	-12.0	-160
20	-20	8.2	7.7	-12.6	-160
	-30	9.9	9.4	-11.6	-160

Table S8. The summarized table of the fitting results (f_a, f_b, f_c, and η) for the parameters of A_-/A_+ and τ_-/τ_+.

	f_a	f_b	f_c	η (°)
A_-	29.1	28.6	-7.8	-115
A_+	47.0	48.0	-14.6	-160
τ_-	172.4ms	175.6ms	-176.2ms	-115
τ_+	353.5ms	346.9ms	-166.9ms	-160

Table S9. The summarized table of the fitting results (y_a, y_b, y_c, and σ) for the parameters of A, W_0, τ, and t_0.

	y_a	y_b	y_c	σ (°)
A	28.6	26.9	-	95
W_0	14.6	14.4	-16.8	-160
τ	230.5ms	225.0ms	-	95
t_0	4.9ms	3.0ms	-	60

Supplementary References

1 X. Zhou, X. Hu, S. Zhou, Q. Zhang, H. Li, T. Zhai, *Adv. Funct. Mater.*, 2017, **27**, 1703858.

2 R. K. Ulaganathan, Y. Lu, C. Kuo, S. R. Tamalampudi, R. Sankar, K. M. Boopathi, A. Anand, K. Yadav, R. J. Mathew, C. Liu, F. C. Chou, Y. Chen, *Nanoscale*, 2016, **8**, 2284-2292

3 Z. Zhou, M. Long, L. Pan, X. Wang, M. Zhong, M. Blei, J. Wang, J. Fang, S. Tongay, W. Hu, J. Li, Z. Wei, *ACS Nano*, 2018, **12**, 12416-12423.

4 S. Zhao, B. Dong, H. Wang, H. Wang, Y. Zhang, Z. V. Han, H. Zhang, *Nanoscale Adv.*, 2020, **2**, 109-139.

5 J. Shim, S. Oh, D. H. Kang, S. Jo, M. H. Ali, W. Choi, K. Heo, J. Jeon, S. Lee, M. Kim, Y. J. Song, J. Park, *Nat. Commun.*, 2016, **7**, 13413.

6 D. Xiang, T. Liu, J. Wang, P. Wang, L. Wang, Y. Zheng, Y. Wang, J. Gao, K. Ang, G. Eda, W. Hu, L. Liu, W. Chen, *Adv. Opt. Mater.*, 2019, **7**, 1901115.

7 E. Zhang, P. Wang, Z. Li, H. Wang, C. Song, C. Huang, Z. G. Chen, L. Yang, K. Zhang, S. Lu, W. Wang, S. Liu, H. Fang, X. Zhou, H. Yan, J. Zou, X. Wan, P. Zhou, W. Hu, F. Xiu, *ACS Nano*, 2016, **10**, 8067-8077.

8 H. Song, T. Li, J. Zhang, Y. Zhou, J. Luo, C. Chen, B. Yang, C. Ge, Y. Wu, J. Tang, *Adv. Mater.*, 2017, **29**, 1700441.

9 J. Lai, X. Liu, J. Ma, Q. Wang, K. Zhang, X. Ren, Y. Liu,Q. Gu, X. Zhuo, W. Lu, Y. Wu, Y. Li, J. Feng, S. Zhou, J. H. Chen, D. Sun, *Adv. Mater.*, 2018, **30**, e1707152.

10 X. Zhou, X. Hu, S. Zhou, Q. Zhang, H. Li, T. Zhai, *Adv. Funct. Mater.*, 2017, **27**, 1703858.